Terr. Atmos. Ocean. Sci., Vol. 28, No. 2, 99-110, April 2017 doi: 10.3319/TAO.2016.09.14.01(EOF5)

# Advanced Ionospheric Probe scientific mission onboard FORMOSAT-5 satellite

Zai-Wun Lin[1], Chi-Kuang Chao[1, 2, *], Jann-Yenq Liu[1, 3], Chien-Ming Huang[1], Yen-Hsyang Chu[1, 3], Ching-Lun Su[1], Ya-Chih Mao[1], and Yeou-Shin Chang[4]

[1] *Graduate Institute of Space Science, National Central University, Taoyuan City, Taiwan*
[2] *Department of Atmospheric Sciences, National Central University, Taoyuan City, Taiwan*
[3] *Center for Space and Remote Sensing Research, National Central University, Taoyuan City, Taiwan*
[4] *National Space Organization, National Applied Research Laboratories, HsinChu, Taiwan*

***Article history:***
Received 13 June 2016
Revised 24 August 2016
Accepted 14 September 2016

***Keywords:***
AIP, FORMOSAT-5, IPEI, ROCSAT-1

***Citation:***
Lin, Z. W., C. K. Chao, J. Y. Liu, C. M. Huang, Y. H. Chu, C. L. Su, Y. C. Mao, and Y. S. Chang, 2017: Advanced Ionospheric Probe scientific mission onboard FORMOSAT-5 satellite. Terr. Atmos. Ocean. Sci., 28, 99-110, doi: 10.3319/TAO.2016.09.14.01(EOF5)

## ABSTRACT

Advanced Ionospheric Probe (AIP) is a piggyback science payload developed by National Central University for FORMOSAT-5 satellite to explore space weather/climate and seismic precursors associated with strong earthquakes. The AIP is an all-in-one plasma sensor that measures ionospheric plasma concentrations, velocities, and temperatures in a time-sharing way and is capable of measuring ionospheric plasma irregularities at a sample rate up to 8192 Hz over a wide range of spatial scales. Electroformed gold grids used in the AIP in theory construct planar electric potential surfaces better than woven grids. Moreover, a plasma injection test performed in the Space Plasma Simulation Chamber has verified that no significant hysteresis is found in current-voltage curves measured by the AIP. It indicates that the AIP can make an accurate measurement of the ionospheric plasma parameters in space. Finally, Ionospheric Plasma and Electrodynamics Instrument (IPEI) observations onboard the ROCSAT-1 satellite are applied to show that the scientific objectives of ionospheric space weather/climate and seismo-ionospheric precursors (SIPs) of the FORMOSAT-5/AIP can be fulfilled. The observations reveal that ion parameter global distributions are helpful in studying the formation and variation in temperature crests and troughs in the 2200 - 2300 local time sector, as well as SIPs in the density and the velocity over the epicenter area, which are anticipated for the FORMOSAT-5 satellite orbit.

## 1. INTRODUCTION

A remote sensing satellite, FORMOSAT-5, is anticipated to launch in 2016 and fly in a 98.28° inclination sun-synchronous circular orbit at 720 km altitude along 1030/2230 local time (LT) sector. Advanced Ionospheric Probe (AIP) as Fig. 1 was proposed by Space Payload Laboratory, Graduate Institute of Space Science, National Central University under an announcement of opportunity for a piggyback science payload of the FORMOSAT-5 satellite and granted by National Space Organization in 2012. The payload was limited in mass under 5 kg, average power per orbit less than 5 W, and lifetime longer than 2 years in mission operation.

The AIP has heritage from past successful missions like Ionospheric Plasma and Electrodynamics Instrument (IPEI) onboard ROCSAT-1 satellite (Yeh et al. 1999) operated during 1999 - 2004, ion probe onboard Sounding Rocket V (Chao et al. 2012) launched on 18 January 2006, and plasma probe onboard Sounding Rocket VII on 5 May 2010. Recently, two AIP sensors were installed on Space Plasma Sensor Package onboard Sounding Rocket IX and have completed a successful flight test on 26 March 2014.

The AIP is basically a multi-grid planar ion probe integrated with a Planar Langmuir Probe (PLP) within a 10 cm × 10 cm aperture as Fig. 2. Unlike the other single-function plasma sensors, the AIP is a software-programmable sensor that plays various roles like PLP, Retarding Potential Analyzer (RPA), and Ion Drift Meter (IDM)/Ion Trap (IT) to

* *Corresponding author*
*E-mail: ckchao@jupiter.ss.ncu.edu.tw*

maximize the total availability of ionospheric plasma concentrations, velocities, and temperatures.

The AIP has another feature in that it measures the total ion concentration at a sample rate up to 8192 Hz. Using this sample rate, fine density structure of the equatorial plasma irregularities can be studied in comparison to the other on-duty plasma sensors like Special Sensor for Ions and Electrons (SSIES) onboard Defense Meteorological Satellite Program (DMSP) satellites at 24 Hz (Rich 1994), decommissioned sensors like IPEI onboard ROCSAT-1 satellite at 1024 Hz (Chang et al. 1999), and Instrument Analyseur Plasma (IAP) onboard Detection of Electro-Magnetic Emissions Transmitted from Earthquake Regions (DEMETER) satellite at 160 Hz (Berthelier et al. 2006).

## 2. SCIENTIFIC OBJECTIVES

The AIP is designed in total availability of ionospheric parameters and high sample rate to study space science like equatorial plasma irregularities, background ionosphere, and ionospheric disturbance caused by geomagnetic storm and earth science like ionospheric perturbations by pre-seismic activities as follows.

### 2.1 Equatorial Plasma Irregularities

One of the most important phenomena in the equatorial ionosphere is the generation of the equatorial spread F (ESF). It is expected that the ESF is related to plasma density irregularity structure caused by initial seeding perturbations from the large-scale gravitational Rayleigh-Taylor instability (Haerendel 1973; Ossakow 1981). The disturbed structure is generated at the bottom side of the F region and can be developed and extended to the topside ionosphere with very large gradient in plasma concentrations. These irregularities can seriously affect the propagation of radio waves over a large range of frequencies. Strong scintillations have been observed from high frequency to GHz frequency range. Therefore, the statistical survey of the global distributions of the ionospheric density irregularities is very important. These patterns have been investigated in a macro-level approach by McClure et al. (1998) with AE-E spacecraft observation and Su et al. (2006) with ROCSAT-1/IPEI data in the last two decades. The FORMOSAT-5/AIP will continue the previous studies to examine the long-term trend of these patterns in this decade.

In a micro-level approach, the AIP is capable of measuring the equatorial plasma irregularities up to 8192 Hz and then analyzing the spectral behaviors on total ion concentration and drift velocity (Su et al. 2001). It may be helpful to re-examine the frozen-in approximation in the ionosphere with the limited regime of scale length between the Boltzmann and non-Boltzmann relations (Chen et al. 2001).

The high-resolution data on the equatorial plasma irregularities could be further applied in ionospheric scintillation forecasting system. For example, a coincident observation that occurred on 24 March 2000 between the plasma irregularities measured by the ROCSAT-1 satellite and a scintillation experiment at the Ascension Island to receive VHF and L-BAND beacon signals from two geosynchronous satellites has been studied for the causal relationship (Liu et al. 2012). The wave amplitude fluctuations have been converted to the ground scintillation sequence in time with an eastward drift velocity of the plasma irregularities derived from the IPEI observation. For a fixed ion density data number, the higher sample rate and eastward drift velocity (~160 m $s^{-1}$) of the plasma irregularities measured in space, the higher time resolution of the converted wave fluctuations at ground

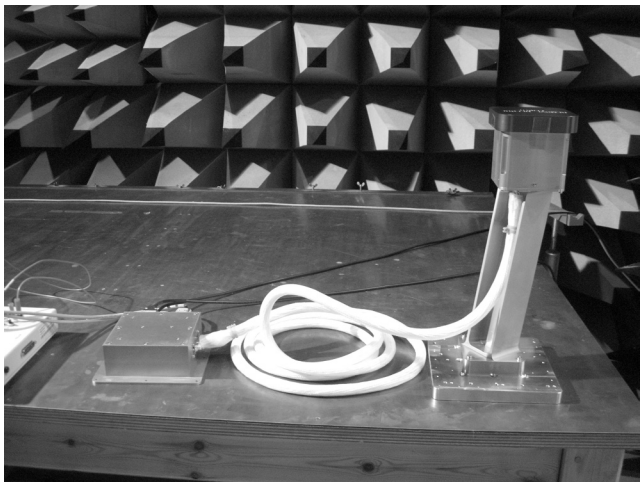

Fig. 1. A photograph of the AIP flight model under electromagnetic compatibility test at National Space Organization. The AIP sensor with a red cover is mounted on a stand in the right to enlarge field of view and a Science Payload Electronics Unit like a metal box in the left to control the sensor operation and communicate with a Command and Data Management Unit.

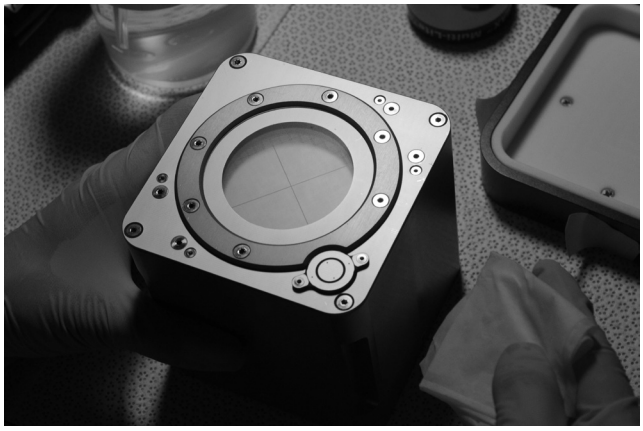

Fig. 2. A photograph of the AIP sensor. The multi-grid ion probe entrance is at the center of the sensor and an electrode with a guarding ring of the Planar Langmuir Probe on the right bottom corner.

and of course the shorter forecast time period is available. However, the FORMOSAT-5 satellite is anticipated for a sun-synchronous orbit of 98° instead of the low-inclination orbit of 35° as the ROCSAT-1 satellite. The similar coincident observation can also be applied and more useful for the ionospheric scintillation forecasting system between high-inclination satellites and ground. The scintillation levels of the other satellite links could be estimated if the plasma irregularities measured by the FORMOSAT-5 satellite appear in the wave propagation paths.

### 2.2 Background Ionosphere

Ion parameter global distributions were derived from the ROCSAT-1 observation and revealed many unique features in various local time sectors, like pre-dawn heating (Chao et al. 2003b, 2010), ion temperature crests in the morning hours (Chao et al. 2004), and movements of the temperature crests in the afternoon sector (Chao et al. 2006), etc. However, lack of electron temperature measurement in the ROCSAT-1 satellite, many temperature features could not be fully understood.

In the early stage of the AIP mission the instrument will be routinely operated within ±75° latitude in the nightside sector (2230 LT sector) to meet a 5-W limit in average power per orbit. Some well-known nighttime ionospheric features like temperature crests and troughs have been detected by the OGO6 (Hanson et al. 1973) and the DMSP spacecraft (Venkatraman and Heelis 1999a) over the last several decades. A model study for the DMSP ion temperature measurement has confirmed that the temperature crests observed at near 15° latitude in the winter hemisphere are due to adiabatic heating and the troughs observed near the magnetic equator are due to adiabatic cooling as plasma is transported along the magnetic field from the summer hemisphere to the winter hemisphere in the nighttime topside ionosphere (Bailey et al. 2000). The upcoming AIP data will make it possible to construct the ion parameter global distributions to investigate the phenomena. Further details will be discussed with the ROCSAT-1/IPEI data set in later paragraphs to investigate the feasibility.

The ion temperature crests were discovered in the dayside sector by the ROCSAT-1 satellite (Chao et al. 2004). The temperature maxima of the ion temperature crests was found located at longitudes of positive magnetic declination in the southern hemisphere during the June solstice and at longitudes of negative magnetic declination in the northern hemisphere during the December solstice. It seems that adiabatic compression heating caused by high downward ion flows plays an important role in forming the crests. However, theoretical models suggested that the temperature crests are mainly related to the heat transfers from electrons, only partially from the adiabatic compression process. The only way to resolve the ambiguity is to install both Langmuir probe and RPA to find out the possible causes.

The AIP is capable of providing complete electron and ion information for the energy exchange study along the 1030 LT sector. A clear understanding of the temperature crests in the morning hours could be revealed in the future. However, it will not be investigated in a regular operation due to the power limit as we mentioned. A special mission operation can be requested to measure the ionospheric parameters in the dayside sector. Nevertheless, the power limit might be removed after an early orbit checkout stage is accomplished. There is still plenty of power reserved in the FORMOSAT-5 satellite mission operation.

### 2.3 Ionospheric Disturbance by Geomagnetic Storm

During geomagnetic storm time, prompt penetration of electric fields and long-lasting disturbance dynamo effect results in large-scale plasma motion in the ionosphere. Greenspan et al. (1991) reported the observation of large density depletion in a narrow longitude near the South Atlantic Anomaly (SAA) region by DMSP F9 satellite at 840 km altitude during the March 1989 magnetic storm. The density depletion was attributed to an enhanced equatorial fountain effect from a locally enhanced eastward electric field near the SAA region related to a large energetic particle precipitation during the storm. It is interesting that similar observations of large density depletion events were again observed during the 6 - 7 April 2000 and the 15 - 16 July 2000 magnetic storms by ROCSAT-1 satellite, at 600 km altitude traversing the magnetic flux tube in the east-west direction. The 15 - 16 July events were reported to correlate with the SAA region (Lin et al. 2001). The large density dropout was further classified by Su et al. (2002) in two groups of ESF plasma irregularities that occurred in either side of the midnight meridian during the storm recovery phase. The two groups of ESF plasma irregularities were both observed in the neighborhood of the SAA region. The FORMOSAT-5/AIP can make a similar observation at 720 km altitude to monitor these plasma disturbances in a very high resolution during the geomagnetic storm. However, it is also noted that such great geomagnetic storms may occur rarely in a solar activity decline phase during the FORMOSAT-5 mission lifetime.

### 2.4 Seismic Precursor

Recently Oyama et al. (2008) examined ionospheric electron temperatures observed by HINOTORI satellite during three earthquakes; M6.6 occurred in November 1981, M7.4 and M6.6 in January 1982 over the Philippines, respectively. It was found that the electron temperature around the epicenters significantly decreased in the afternoon periods within 5 days before and after the three earthquakes. The AIP has a great advantage in measuring electron temperature

but also more ion parameters will be cross-checked for possible mechanism correlation. Meanwhile, the FORMOSAT-5 satellite will pass over Taiwan every two days and the AIP can also collaborate with integrated Study for Taiwan Earthquake Precursors (iSTEP) to survey all possible earthquake precursors for disaster reduction (Liu et al. 2016).

To see whether FORMOSAT-5/AIP can be used to detect seismo-ionospheric precursors (SIPs) or not, ion density, temperature, and velocity probed by ROCSAT-1/IPEI have been examined as well as the global ionospheric map (GIM) of the total electron content (TEC) derived by ground-based GPS receivers during the 31 March 2002 M6.8 Earthquake in Taiwan (Liu and Chao 2017). The anomalous decreases in the ROCSAT-1/IPEI ion density and the GIM TEC concurrently appear around the epicenter area 1 - 5 days before the earthquake, which suggests that FORMOSAT-5/AIP can be used to detect SIPs.

## 3. PRINCIPLES OF MEASUREMENT

The AIP is an all-in-one plasma sensor to measure all the characteristics of the ionospheric plasma in different operation modes like the PLP, RPA, and IDM/IT but in a time-sharing way.

### 3.1 PLP

When the AIP operates in the PLP mode, the PLP electrode (shown in the left of the Fig. 3) is applied to a sweeping voltage between -10 and +10 V and isolated from aperture plane. Once the sweeping voltage is lower than plasma potential, the electrode repels electrons, and accelerates ions. As the voltage decreases, electron current decreases rapidly. The electron temperature ($T_e$) can be determined by the slope of the current-voltage (I-V) curve (Boyd 1968) as shown in Eq. (1),

$$\frac{\kappa T_e}{e} = \frac{1}{\frac{d}{dV}[\ln(I)]} \tag{1}$$

where $I$ is the total electric current through the PLP electrode, $V$ is the sweeping voltage applied to the PLP electrode, $\kappa$ is the Boltzmann constant, $e$ is the electron charge. As the slope of the I-V curve is flat, the $T_e$ is higher. As the slope is steep, the $T_e$ is lower.

### 3.2 RPA

The AIP multi-grid ion probe consists of four high-transparent electroformed gold grids to manage incoming plasma, as shown in Fig. 3. The first dual grids, G1, are aperture grids arranged in front of the probe and connected to a floating potential device that allow the incoming plasma to flow smoothly into the probe without interference from the transverse electric field. The second grid, G2, is a retarding grid connected to a programmable sweeping retarding voltage circuit between -10 and +10 V. The grid forms an electric potential barrier to block low energy positive ions from the probe. The third grid, G3, is a suppressor grid maintained at -15 V to repel the incoming electrons into a quadrant gold-coating collector and also reduces the amount of photoelectrons escaping from the collector when the sunrays strike the collector. All four quadrant collector gold-coating plates are maintained at the floating potential and programmable to connect with an ammeter or individual ammeters via an analog switch.

In the RPA mode, positive ions with low kinetic energy are repelled out of the probe or neutralized by the grids and probe interior boundary as the retarding voltage increases. Positive ions with high kinetic energy can penetrate through the retarding grid to the collector if they do not contact the suppressor grid or the interior probe boundary. The higher the retarding voltage, the lower the current measured at the collector. Such a sampling process can be recorded as the I-V curves to derive the ion temperature, composition, and ion ram speed. A 1-dimensional ion current equation (Whipple 1961; Heelis and Hanson 1998) for this application is written in Eq. (2),

$$I(V) = A\sum_i q_i N_i U_i \frac{1}{2}\left[1 + erf(\beta_i F_i) + \frac{\exp(-\beta_i^2 F_i^2)}{\sqrt{\pi}\,\beta_i U_i}\right],$$
$$\beta_i = \sqrt{\frac{M_i}{2\kappa T_i}}, \text{ and } F_i = U_i - \sqrt{\frac{2q_i V}{M_i}} \tag{2}$$

where $I$ is the ion current measured at the collector, $q_i$ is the electric charge for species $i$, $A$ is the effective collection area, $N_i$ is the ion concentration for species $i$, $U_i$ is the ion ram speed for species $i$, $M_i$ is the ion mass for species $i$, $\kappa$ is the Boltzmann constant, $T_i$ is the ion temperature for species $i$, $V$ is the maximum electric potential along the path for plasma from outside environment to the probe (sometimes can be simplified as retarding potential). The electric potential is referenced to far-away plasma and it is assumed that the electric potential of the far-away plasma is zero. It is also noted that a numerical model to estimate the effects of grid alignment (Chao and Su 2000) and electric potential depression on the grids (Chao et al. 2003a) is required to derive the precise $T_i$ and $U_i$.

### 3.3 IDM/IT

In the IDM/IT mode G1 and the G2 are maintained at the floating potential. In the IT mode all the four quadrant collector gold-coating plates are connected together with an ammeter. In the IDM mode all the plates are connected with individual ammeters. The incoming ion arrival angles can be

estimated from ion current differences in the adjacent ammeters, as shown in Fig. 4. The arrival angle, $\alpha$, of the incoming ion for a circular aperture opening is expressed in Eq. (3),

$$\alpha = \tan^{-1}\left[\left(\frac{W}{2D}\right)\cos\frac{\theta}{2}\right] \text{ and } \theta = \sin\theta + \left[1 - \left(\frac{I_1 - I_2}{I_1 + I_2}\right)\right]\pi \quad (3)$$

where $W$ is the width of the aperture, $D$ is the depth between the aperture and the collector. The immediate parameter $\theta$ must be solved by numerical methods, e.g., fixed-point iteration (Kreyszig 2011). Note that the formula is a new starting point for a drift meter to use the circular aperture opening instead of the square aperture opening as before (Heelis and Hanson 1998).

### 3.4 Geophysical Parameters

The AIP can be configured to measure ambient plasma at three sample rates, NORMAL mode operating at 128 Hz, FAST mode at 1024 Hz, and BURST mode at 8192 Hz. By default, the AIP is set to PRI (an initial point for PLP-RPA-IDM/IT) mode to measure ionospheric plasma in a PLP, RPA, and IDM/IT cycle mode at one second each sequentially. Therefore, it must be assumed that all ionospheric parameters have a slow temporal variation within 3 sec as shown in Table 1 and are uniform within 22.5 km in spatial scale (if the satellite speed is 7.5 km $s^{-1}$). After one cycle is complete, the geophysical parameters, $N_i$, $V_i$, $T_i$, and $T_e$, can be derived from the steps shown in Fig. 5. The AIP can also run PLP, RPA, or IDM/IT solely to increase the data rates for specific parameters as shown in Table 1, but this leads to an incomplete data set.

The PLP mode can obtain $T_e$ directly. $T_e$ will be used to estimate floating potential (Zuccaro and Holt 1982) obtain retarding potentials (referenced to plasma potential) with the retarding voltages (referenced to floating potential). The RPA mode can obtain $T_i$, $U_i$, and $C_i$ (composition ratio for species $i$ to total ions). The IDM/IT mode can obtain the total ion flux and further convert to $N_i$ with $T_i$ , $U_i$, and $C_i$, but also obtain two arrival angles, $\alpha_H$ and $\alpha_V$, and convert them to $V_i$ with $U_i$.

Under the FORMOSAT-5 satellite orbits the geophysical measurement requirements are derived from the International Reference Ionosphere model (Bilitza 2001) and listed in Table 2. The AIP is designed to outperform the geophysical measurement requirements of the FORMOSAT-5 satellite and its performance capabilities are listed in Table 3 for references.

## 4. EVALUATION ON HYSTERESIS IN I-V CURVES

The "hysteresis" phenomenon in Langmuir probe I-V characteristics was observed by Wehner and Medicus (1952) that the I-V curve collected by probe voltage ramp up is different from that by ramp down. The hysteresis is attributed to electrode surface contamination and can be reduced using a clean probe (Smith 1972) or by a rapid sweep of the probe voltage (Oyama 1976). Moreover, this is not just found in the Langmuir probe, it also happens to a multi-grid RPA that measures ion temperature (Minami et al. 1980). The plasma temperature cannot be correctly determined if significant hysteresis is shown in the I-V curve.

From the measurement principles, the grids inside the ion probe are used to provide electric potential surface to filter out unwanted charged particles. In the past, woven stainless steel grids were used, like the ion probe for the Sounding Rocket V and plasma probe for the Sounding Rocket VII. Sometimes the grids are gold coated, as in ROCSAT-1/IPEI. The AIP uses electroformed gold grids to ensure better structure and strength in addition to higher transparency. In theory the electroformed grids can approximate ideal electric potential surfaces better than the woven grids for the same wire diameter and mesh density.

Meanwhile, laboratory simulation has been performed on an AIP prototype in Space Plasma Simulation Chamber (Chao et al. 2012). Two I-V curves were measured by the AIP for retarding G2 sweeping up and down voltage in

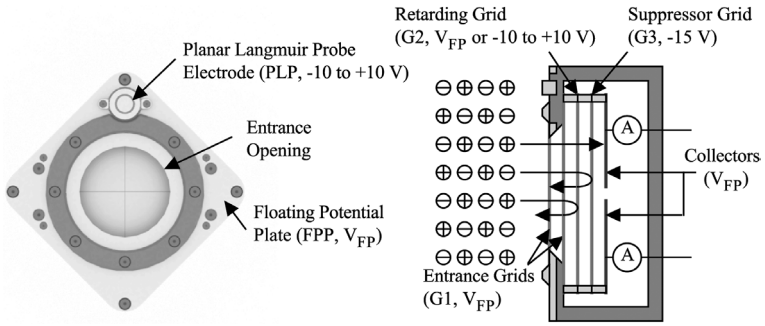


Fig. 3. An illustration of the AIP to operate in the RPA mode. Positive ions with low incoming kinetic energy are repelled by a retarding grid biased at a voltage higher than plasma potential, but positive ions with high kinetic energy can penetrate through the retarding grid to the collector. Electrons are all repelled by a suppressor grids biased in -15 V.

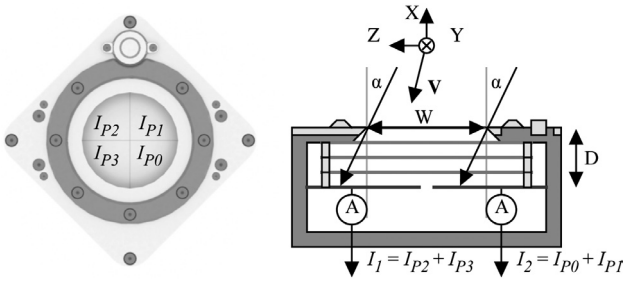


Fig. 4. An illustration of the AIP to operate in the IDM mode.

Table 1. AIP Data Rates for All Parameters.

| Mode | IT ($N_i$) | IDM ($\alpha_H$ and $\alpha_V$) | PLP ($T_e$) or RPA ($T_i, C_i, U_i$) | PRI ($T_e, T_i, C_i, V_i, N_i$) |
|---|---|---|---|---|
| NORMAL | 128 Hz | 32 Hz | 1 Hz | 1/3 Hz |
| FAST | 1024 Hz | 256 Hz | 1 Hz | 1/3 Hz |
| BURST | 8192 Hz | 2048 Hz | 1 Hz | 1/3 Hz |

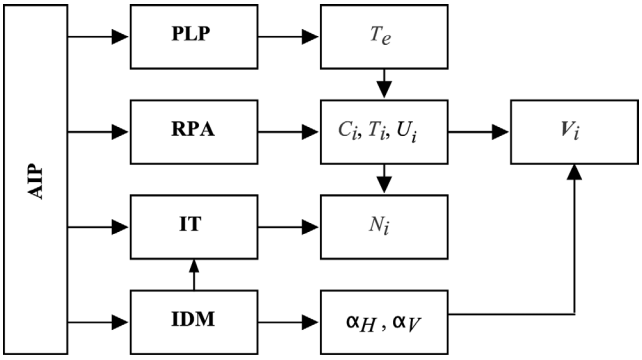


Fig. 5. Geophysical ionospheric parameters derived from the AIP operation under PLP, RPA, and IDM/IT.

Table 2. FORMOSAT-5 Geophysical Measurement Requirements.

| Parameters | Range | Sensitivity | Accuracy |
|---|---|---|---|
| $C_i$ | 5 - 100% | 1% | 10% |
| $N_i$ | $10^3$ to $5 \times 10^6$ cm$^{-3}$ | 1% | 10% |
| $\boldsymbol{V}_i$ | ±2 km s$^{-1}$ (cross track)<br>±2 km s$^{-1}$ (ram) | ±10 m s$^{-1}$<br>±100 m s$^{-1}$ | ±50 m s$^{-1}$<br>±200 m s$^{-1}$ |
| $T_i$ | 750 - 5000 K | ±50 K | ±200 K |
| $T_e$ | 750 - 5000 K | ±50 K | ±200 K |

Table 3. AIP Performance Capabilities.

| Parameters | Range | Sensitivity | Accuracy |
|---|---|---|---|
| $C_i$ | 3 - 100% | 1% | 10% |
| $N_i$ | $4 \times 10^2$ to $1.2 \times 10^7$ cm$^{-3}$ | 1% | 10% |
| $\boldsymbol{V}_i$ | ±3.2 km s$^{-1}$ (cross track)<br>±5 km s$^{-1}$ (ram) | ±10 m s$^{-1}$<br>±100 m s$^{-1}$ | ±50 m s$^{-1}$<br>±200 m s$^{-1}$ |
| $T_i$ | 500 - 10000 K | ±50 K | ±200 K |
| $T_e$ | 500 - 10000 K | ±50 K | ±200 K |

Fig. 6 to verify the AIP measurement accuracy. It is clear that the two curves are almost identical and implies that the AIP electroformed gold grids can greatly reduce hysteresis in the measured I-V curves. Note also that the derived ion temperature is about 540 K using a grid-search curve fitting scheme (Bevington and Robinson 2003).

## 5. EXAMPLES USING ROCSAT-1/IPEI

The IPEI onboard the ROCSAT-1 satellite consists of an IT to collect ion fluxes, a pair of drift meters to measure the arrival angles of the ion flow, and a RPA to obtain current-voltage curves for ion temperature, ion composition, and ram flow analyses. The FORMOSAT-5/AIP can measure entire ion parameters provided by the ROCSAT-1/IPEI but in a higher orbit at 720 km altitude and a wider coverage in latitude. Therefore, in this example global ion parameter distributions derived by the ROCSAT-1/IPEI are used to determine if the FORMOSAT-5/AIP can be applied to study nighttime ion temperature crests and troughs caused by adiabatic plasma heating and cooling processes, respectively.

The ROCSAT-1 satellite had a 600-km circular orbit with a 35° inclination and can be used to study seasonal variations adequately in the low- to mid-latitude region since the satellite presents a 52-day re-visiting period. Statistical averages of the seasonal, diurnal, longitudinal, and latitudinal variations in the topside ionospheric ion parameters from 5 February 2000 to 4 February 2001 have been constructed at 30° intervals in geographic longitude (GLON), at 5° intervals in geographic latitude (GLAT), and at 1-hr interval in local LT under a quiet time condition of geomagnetic index $K_p$ less than 3. Global ion parameter distributions in the 2200 - 2300 LT are further examined in Fig. 7. The plots are arranged in columns from left to right for (a) ion temperature ($T_i$), (b) field-aligned ion flow ($V_{\|}$), (c) $O^+$ percentage, and (d) total ion concentration ($N_i$). Seasonal variation is arranged in panels from top to bottom for the March equinox, the June solstice, the September equinox, and the December solstice with average solar flux $F_{10.7}$ varied from 188, 189, 169, and 172 ($\times 10^{-22}$ W m$^{-2}$ Hz$^{-1}$), respectively. A thick green line is drawn in each panel to indicate the magnetic dip equator obtained by the International Geomagnetic Reference Field model (Tsyganenko 1995). Here a geographic coordinate system is used but the dip latitude (DLAT) of a geomagnetic coordinate will also be noted in the article.

From Fig. 7a, all of the $T_i$ distributions show low temperature near the dip equator and high temperature at higher latitudes. The distributions are almost symmetrical with respect to the dip latitudes during the equinoxes but are noted asymmetrical in both hemispheres during the solstices. For convenience, the low temperature region near the dip equator is called $T_i$ troughs. During the equinoxes, centers of the $T_i$ troughs are almost located at the dip equator. The average temperature of the $T_i$ troughs is about 945 K during the March equinox and 900 K during the September equinox. During the solstices, centers of the $T_i$ troughs shift away from the dip equator to summer hemisphere for most longitudes. The average temperature of the $T_i$ troughs is about 850 K during the June solstice and 910 K during the December solstice. The regions of the $T_i$ troughs under the average temperature are shown at 0 < DLAT < 10°N between 270° and 150°E during the June solstice and at 0 < DLAT < 10°S between 0° and 270°E during the December solstice.

In contrast, a high temperature region (> 1050 K) can also be found at 15° < DLAT < 25° for most longitudes in the winter hemisphere and is called $T_i$ crests. During the June solstice, the most significant $T_i$ crest is located at negative magnetic declination (DECL) between 300° and 360°E (or called it the South Atlantic region). $T_i$ maximum (~1120 K) of the $T_i$ crest is found at 22.5°S and 315°E (-16.8°S in DLAT and -17.5° in DECL). During the December solstice, the $T_i$ crest is located at positive magnetic declination between 180° and 270°E (or called it the North Pacific region). $T_i$ maximum (~1080 K) of the $T_i$ crest is located at 12.5°N and 255°E (~20.6°N in DLAT and 7.80°N in DECL).

It is well known that nighttime topside $T_i$ at low latitudes is greatly affected by field-aligned inter-hemispheric plasma flows (Venkatraman and Heelis 1999a). The $T_i$ troughs in the summer hemisphere and crests in the winter hemisphere are recognized as convective expansion and compression of ions, respectively, along a field line by the field-aligned inter-hemispheric plasma flows (Bailey et al. 1973). The $V_{\|}$ in the Fig. 7b can be used to examine the corresponding $T_i$ distributions. The $V_{\|}$ directed parallel to the field line (northward) is shown in red color and anti-parallel (southward) in blue. The $V_{\|}$ shows a higher flow speed in the winter hemisphere during the solstices than those during the equinoxes. During the June solstice, the anti-parallel $V_{\|}$ larger than 150 m s$^{-1}$ are located at 15°S < DLAT < 40°S between 300° and 90°E. During the December solstice, the parallel $V_{\|}$ larger than 100 m s$^{-1}$ are located between 10°N < DLAT < 20°N between 150° and 270°E. The $V_{\|}$ distributions can be understood qualitatively by neutral wind patterns. Zonal winds are directed in the eastward direction (Blum and Harris 1975) and meridional winds are mostly directed from summer to winter hemisphere during the solstices.

However, the ion cooling and heating efficiencies caused by the convective expansion and compression are strongly related to the $O^+$ percentage. Since $O^+$ has a smaller scale height than $H^+$, the plasma quasi-adiabatic expansion is more efficient below the $O^+$-$H^+$ transition height when $O^+$ is the dominant ion species (Venkatraman and Heelis 1999b). The $O^+$ percentage is shown in Fig. 7c and the $N_i$ is listed in Fig. 7d. During the equinoxes, the $O^+$ percentage (~85% for the March equinox and up to 58% for the September equinox) and $N_i$ (~$10^5$ # cm$^{-3}$ for March equinox and down

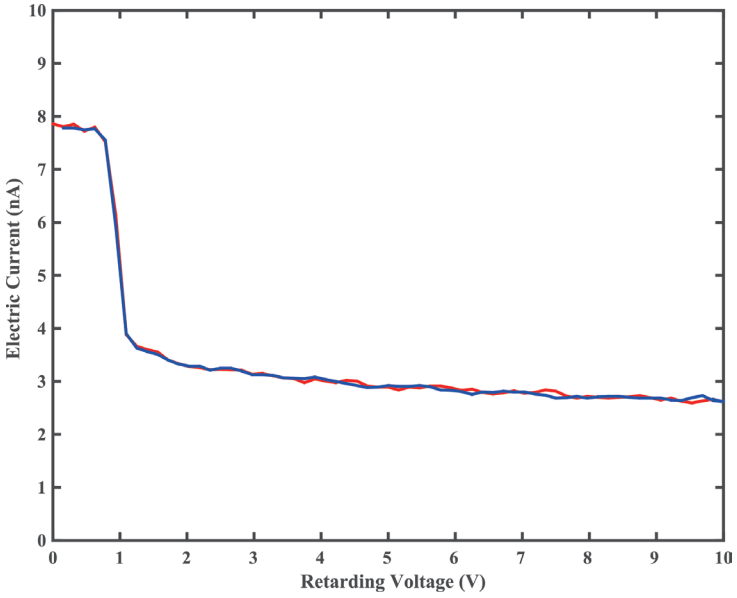


Fig. 6. Two electric current-voltage curves measured by an AIP prototype in a plasma injection test. The red line indicates the electric current measured when the retarding voltage of the G2 is sweeping up and the blue line when the retarding voltage is sweeping down.

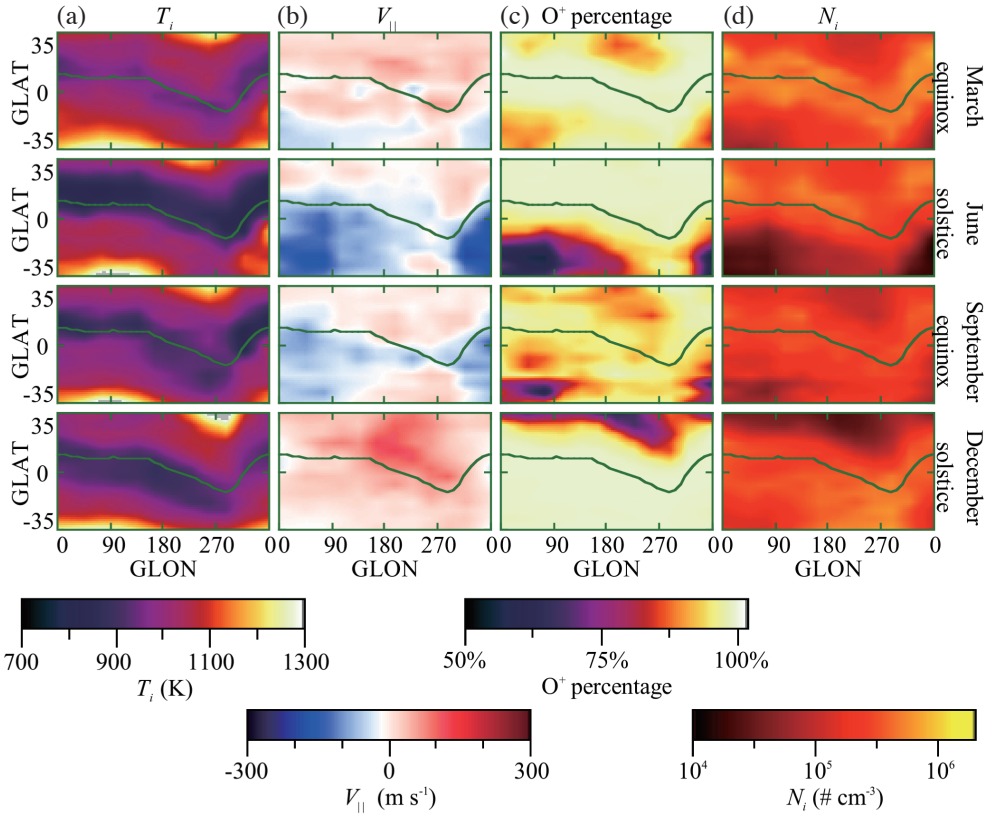


Fig. 7. Ion parameter global distributions from the ROCSAT-1 satellite observation for geographic longitude (GLON) versus geographic latitude (GLAT) in year 2000 - 2001. The plots are arranged in columns from left to right for (a) $T_i$, (b) $V_{||}$, (c) $O^+$ percentage, and (d) $N_i$ in the 2200 - 2300 LT sector. The plots are arranged from top to bottom for the March solstice, the June solstice, the September equinox, and the December solstice. A thick green line is drawn in each panel to indicate the magnetic dip equator. $V_{||}$ directed parallel to the field line (northward) is shown in red color and anti-parallel to the field line (southward) in blue.

to $5 \times 10^4$ # $cm^{-3}$ for the September equinox) are slightly low at higher dip latitudes in the North Pacific region and in the South Atlantic and South African region. During the June solstice, the $O^+$ percentage (< 75%) and $N_i$ (< $4 \times 10^4$ # $cm^{-3}$) are significant low at DLAT > 25°S between 330° and 150°E. During the December solstice, the $O^+$ percentage (< 75%) and $N_i$ (< $4 \times 10^4$ # $cm^{-3}$) are also significant low at DLAT > 25°N between 180° and 270°E. The distributions are mainly caused by the downward $V_{||}$ to reduce the $O^+$ percentage and $N_i$ greatly.

The high $V_{||}$ observed at negative magnetic declination longitudes during the June solstice and at positive magnetic declination longitudes during the December solstice are possible to form the $T_i$ troughs located in the summer hemisphere but close to the dip equator via the adiabatic expansion process. The high $V_{||}$ will also form the $T_i$ crests in the winter hemisphere but limited to the low $O^+$ percentage boundary via the adiabatic compression process. FORMOSAT-5 is anticipating flying at 720 km altitude that is just between the ROCSAT-1 satellite at 600 km altitude and DMSP-series satellites at ~840 km altitude. It is helpful to investigate the formation and variation of the $T_i$ troughs and crests in the low-latitude region after the data acquisition of the FORMOSAT-5/AIP.

SIPs associated with large earthquakes have been studied for more than three decades (cf. Hayakawa and Fujinawa 1994; Hayakawa 1999; Liu et al. 2000; Hayakawa and Molchanov 2002; Pulinets and Boyarchuk 2005). The short comings of these studies included they were conducted in very limited areas and mainly over the land. By contrast, the satellite observation provides a large coverage over both land and sea. Liu et al. (2001) pioneer using the TEC derived from a local network of ground-based GPS receivers to detect SIPs appearing 1, 3, and 4 days before the 21 September 1999 M7.6 Chi-Chi earthquake. Many event studies and statistical analyses on SIPs of the GPS TEC related to large earthquakes in Taiwan have been carried out (Chen et al. 2004; Kamogawa et al. 2004; Liu et al. 2004a, b, 2006, 2008, 2010a; Tsai et al. 2004; Saroso et al. 2008; Nishihashi et al. 2009). Following that, the global ionosphere map of the GPS TEC has been used to globally study SIPs appearing few days before the 26 December 2004 M9.3 Sumatra-Andaman Earthquake (Liu et al. 2010b), the 11 May 2008 M8.0 Wenchuan earthquake (Liu et al. 2009, 2015), and the 12 January 2010 M7.0 Haiti earthquake (Liu et al. 2011). These GPS TEC studies show that the ionospheric plasma, electron density and/or ion density, is sensitive to detect SIPs.

Here, the ion density probed by ROCSAT-1/IPEI is used to demonstrate detecting SIPs associated with the 31 March (331) 2002 M6.8 Earthquake occurring at Yilan, Taiwan. Kamogawa et al. (2004) reported that the ionospheric TEC derived from a local network of ground-based GPS receivers significantly decreased 2, 4, and 5 days before the 331 Yilan earthquake. Meanwhile, statistical results show that the ionospheric electron density and the GPS TEC tended to decrease significantly in the afternoon/evening periods 1 - 6 days before large earthquakes in Taiwan (Liu et al. 2004a).

Based on the quasi-neutrality of plasma, the ROCSAT-1/IPEI ion density would be a suitable and sensitive parameter to detect SIPs. To detect the spatial distribution of SIPs, the ion density observed in the afternoon and evening periods in Taiwan (i.e., 06:00 - 16:00UT) 45 days before to after the earthquake are constructed as a reference. We then examine the differences in corresponding reference subtracting from the observations 6 - 10, 1 - 5 days before and 1 - 5, 6 - 10 days after the earthquake, respectively. Figure 8 displays that the ion density around the epicenter area (15 - 30°N, 110 - 140°E) significantly decreased 1 - 5 days before and after the Yilan earthquake, which generally agree with the local ground-based GPS TEC decreasing significantly 2, 4, and 5 day before the earthquake as reported by Kamogawa et al. (2004), as well as the SIPs of the GIM TEC specifically appear over the epicenter 1 - 5 days before, especially on 29 March 2002 (2 days before), the earthquake reached by Liu et al. (2016). Nevertheless, these agreements suggest that FORMOSAT-5/AIP can be applied to detect SIPs of worldwide large earthquakes.

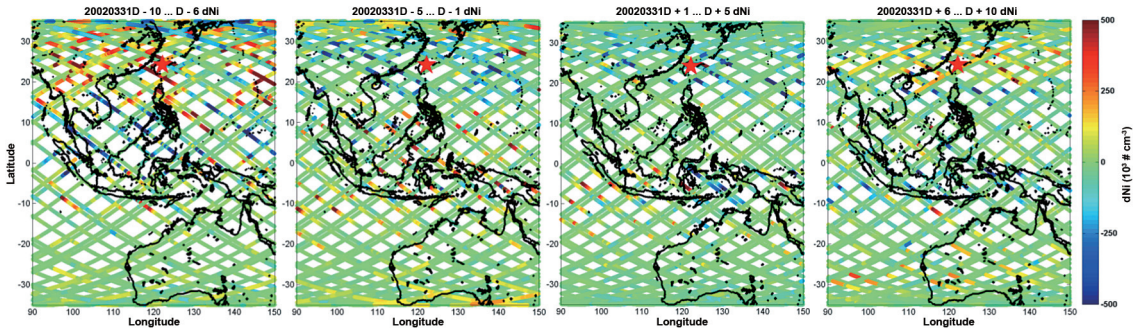


Fig. 8. Total ion concentration difference ($\Delta N_i$) observed by the ROCSAT-1/IPEI during the 31 March 2002 M6.8 Yilan earthquake. The measured $\Delta N_i$ along the satellite tracks for 6 - 10 days before, 1 - 5 days before, 1 - 5 days after, and 6 - 10 days after the earthquake are shown from left to right. The star that marks in each panel indicates the epicenter of the earthquake.

## 6. SUMMARY

The AIP is designed to maximize total availability in ionospheric plasma parameters and sample rates to meet the scientific objectives. The I-V curves measured by the AIP in the plasma injection test indicated that the sensor is almost free of contamination. The AIP could obtain accurate and complete ionospheric plasma parameters for scientific research and application. The scientific objectives outlined in this article will be clarified in the future.

Once comprehensive dataset is available from the AIP, a systematic examination of longitudinal and seasonal variations in the ionospheric parameters in the topside F region can be conducted for all latitudinal coverage like the temperature crests and troughs example. The transient and long-term variations in ionospheric plasma can be monitored in a solar activity decline phase and benefit the public and scientists interested in space weather/climate as well as the seismic precursors associated with strong earthquakes.

**Acknowledgements** This work was supported by grant NSPO-S-100005 National Space Organization, National Applied Research Laboratories and MOST102-2119-M-008-011 and MOST105-2119-M-008-024 Ministry of Science and Technology, Taiwan, ROC.

## REFERENCES

Bailey, G. J., R. J. Moffett, W. B. Hanson, and S. Sanatani, 1973: Effects of interhemisphere transport on plasma temperatures at low latitudes. *J. Geophys. Res.*, **78**, 5597-5610, doi: 10.1029/JA078i025p05597. [Link]

Bailey, G. J., M. H. Denton, R. A. Heelis, and S. Venkatraman, 2000: A modelling study of the latitudinal variations in the nighttime plasma temperatures of the equatorial topside ionosphere during northern winter at solar maximum. *Ann. Geophys.*, **18**, 1435-1446, doi: 10.1007/s00585-000-1435-6. [Link]

Berthelier, J. J., M. Godefroy, F. Leblanc, E. Seran, D. Peschard, P. Gilbert, and J. Artru, 2006: IAP, the thermal plasma analyzer on DEMETER. *Planet. Space Sci.*, **54**, 487-501 doi: 10.1016/j.pss.2005.10.018. [Link]

Bevington, P. R. and D. K. Robinson, 2003: Data Reduction and Error Analysis for the Physical Sciences, McGraw-Hill, 320 pp.

Bilitza, D., 2001: International Reference Ionosphere 2000. *Radio Sci.*, **36**, 261-275, doi: 10.1029/2000RS002432. [Link]

Blum, P. W. and I. Harris, 1975: Full non-linear treatment of the global thermospheric wind system—II. Results and comparison with observations. *J. Atmos. Terr. Phys.*, **37**, 213-235, doi: 10.1016/0021-9169(75)90107-5. [Link]

Boyd, R. L. F., 1968: Langmuir probes on spacecraft. In: Richter, J. (Ed.), Plasma Diagnostics, North-Holland Publishing Co., Amsterdam, 732-776.

Chang, Y. S., W. L. Chiang, S. J. Ying, B. J. Holt, C. R. Lippincott, and K. C. Hsieh, 1999: System architecture of the IPEI payload on ROCSAT-1. *Terr. Atmos. Ocean. Sci.*, Supplementary Issue, 7-18, doi: 10.3319/TAO.1999.10.S.7(ROCSAT). [Link]

Chao, C. K. and S. Y. Su, 2000: Charged particle motion inside the retarding potential analyzer. *Phys. Plasmas*, **7**, 101-107, doi: 10.1063/1.873817. [Link]

Chao, C. K., S. Y. Su, and H. C. Yeh, 2003a: Grid effects on the derived ion temperature and ram velocity from the simulated results of the retarding potential analyzer data. *Adv. Space Res.*, **32**, 2361-2366, doi: 10.1016/S0273-1177(03)90566-7. [Link]

Chao, C. K., S. Y. Su, and H. C. Yeh, 2003b: Presunrise ion temperature enhancement observed at 600 km low- and mid-latitude ionosphere. *Geophys. Res. Lett.*, **30**, doi: 10.1029/2002GL016268. [Link]

Chao, C. K., S. Y. Su, and H. C. Yeh, 2004: Ion temperature crests and troughs in the morning sector of the low-latitude and midlatitude topside ionosphere. *J. Geophys. Res.*, **109**, A11303, doi: 10.1029/2003JA010360. [Link]

Chao, C. K., S. Y. Su, and H. C. Yeh, 2006: Ion temperature variation observed by ROCSAT-1 satellite in the afternoon sector and its comparison with IRI-2001 model. *Adv. Space Res.*, **37**, 879-884, doi: 10.1016/j.asr.2005.06.071. [Link]

Chao, C. K., S. Y. Su, J. D. Huba, and K. I. Oyama, 2010: Modeling the presunrise plasma heating in the low- to midlatitude topside ionospheres. *J. Geophys. Res.*, **115**, A09304, doi: 10.1029/2009JA014923. [Link]

Chao, C. K., Y. H. Chu, C. L. Su, and S. Minami, 2012: In-situ measurement of ionospheric E-region plasma irregularities over Taiwan. *Terr. Atmos. Ocean. Sci.*, **23**, 333-342, doi: 10.3319/TAO.2011.12.23.01(AA). [Link]

Chen, K. Y., H. C. Yeh, S. Y. Su, C. H. Liu, and N. E. Huang, 2001: Anatomy of plasma structures in an equatorial spread F event. *Geophys. Res. Lett.*, **28**, 3107-3110, doi: 10.1029/2000GL012805. [Link]

Chen, Y. I., J. Y. Liu, Y. B. Tsai, and C. S. Chen, 2004: Statistical tests for pre-earthquake ionospheric anomaly. *Terr. Atmos. Ocean. Sci.*, **15**, 385-396, doi: 10.3319/TAO.2004.15.3.385(EP). [Link]

Greenspan, M. E., C. E. Rasmussen, W. J. Burke, and M. A. Abdu, 1991: Equatorial density depletions observed at 840 km during the great magnetic storm of March 1989. *J. Geophys. Res.*, **96**, 13931-13942, doi: 10.1029/91JA01264. [Link]

Haerendel, G. E., 1973: Theory of equatorial spread-F. Report, Maxplanck-Institut fur Extraterre. Phys., Garching, Germany.

Hanson, W. B., A. F. Nagy, and R. J. Moffett, 1973: Ogo 6 measurements of supercooled plasma in the equatorial exosphere. *J. Geophys. Res.*, **78**, 751-756, doi: 10.1029/JA078i004p00751. [Link]

Hayakawa, M., 1999: Atmospheric and Ionospheric Electromagnetic Phenomena Associated with Earthquakes, Terra Scientific Publishing Company, Tokyo, 996 pp.

Hayakawa, M. and Y. Fujinawa, 1994: Electromagnetic Phenomena Related to Earthquake Prediction, Terra Scientific Publishing Company, Tokyo, 667 pp.

Hayakawa, M. and O. A. Molchanov, 2002: Seismo Electromagnetics: Lithosphere-Atmosphere-Ionosphere Coupling, Terra Scientific Publishing Company, Tokyo, 477 pp.

Heelis, R. A. and W. B. Hanson, 1998: Measurements of thermal ion drift velocity and temperature using planar sensors. In: Pfaff, R. F., J. E. Borovsky, and D. T. Young (Eds.), Measurement Techniques in Space Plasmas: Particles, American Geophysical Union, Washington, D.C., 61-71, doi: 10.1029/GM102p0061. [Link]

Kamogawa, M., J. Y. Liu, H. Fujiwara, Y. J. Chuo, Y. B. Tsai, K. Hattori, T. Nagao, S. Uyeda, and Y. H. Ohtsuki, 2004: Atmospheric field variations before the March 31, 2002 *M*6.8 earthquake in Taiwan. *Terr. Atmos. Ocean. Sci.*, **15**, 397-412, doi: 10.3319/TAO.2004.15.3.397(EP). [Link]

Kreyszig, E., 2011: Advanced Engineering Mathematics, Wiley, 1280 pp.

Lin, C. S., H. C. Yeh, and S. Y. Su, 2001: ROCSAT-1 satellite observations of magnetic anomaly density structures during the great magnetic storm of July 15-16, 2000. *Terr. Atmos. Ocean. Sci.*, **12**, 567-582, doi: 10.3319/TAO.2001.12.3.567(A). [Link]

Liu, J. Y. and C. K. Chao, 2017: An observing system simulation experiment for FORMOSAT-5/AIP detecting seismo-ionospheric precursors. *Terr. Atmos. Ocean. Sci.*, **28**, 117-127, doi: 10.3319/TAO.2016.07.18.01(EOF5). [Link]

Liu, J. Y., Y. I. Chen, S. A. Pulinets, Y. B. Tsai, and Y. J. Chuo, 2000: Seismo-ionospheric signatures prior to M≥6.0 Taiwan earthquakes. *Geophys. Res. Lett.*, **27**, 3113-3116, doi: 10.1029/2000GL011395. [Link]

Liu, J. Y., Y. I. Chen, Y. J. Chuo, and H. F. Tsai, 2001: Variations of ionospheric total electron content during the Chi-Chi Earthquake. *Geophys. Res. Lett.*, **28**, 1383-1386, doi: 10.1029/2000GL012511. [Link]

Liu, J. Y., Y. J. Chuo, S. J. Shan, Y. B. Tsai, Y. I. Chen, S. A. Pulinets, and S. B. Yu, 2004a: Pre-earthquake ionospheric anomalies registered by continuous GPS TEC measurements. *Ann. Geophys.*, **22**, 1585-1593, doi: 10.5194/angeo-22-1585-2004. [Link]

Liu, J. Y., Y. I. Chen, H. K. Jhuang, and Y. H. Lin, 2004b: Ionospheric foF2 and TEC anomalous days associated with M ≥ 5.0 earthquakes in Taiwan during 1997-1999. *Terr. Atmos. Ocean. Sci.*, **15**, 371-383, doi: 10.3319/TAO.2004.15.3.371(EP). [Link]

Liu, J. Y., Y. I. Chen, Y. J. Chuo, and C. S. Chen, 2006: A statistical investigation of preearthquake ionospheric anomaly. *J. Geophys. Res.*, **111**, A05304, doi: 10.1029/2005JA011333. [Link]

Liu, J. Y., S. W. Chen, Y. C. Chen, H. Y. Yen, C. P. Chang, W. Y. Chang, L. C. Tsai, C. H. Chen, and W. H. Yang, 2008: Seismo-ionospheric precursors of the 26 December 2006 M 7.0 Pingtung earthquake doublet. *Terr. Atmos. Ocean. Sci.*, **19**, 751-759, 2008, doi: 10.3319/TAO.2008.19.6.751(PT). [Link]

Liu, J. Y., Y. I. Chen, C. H. Chen, C. Y. Liu, C. Y. Chen, M. Nishihashi, J. Z. Li, Y. Q. Xia, K. I. Oyama, K. Hattori, and C. H. Lin, 2009: Seismoionospheric GPS total electron content anomalies observed before the 12 May 2008 $M_w$7.9 Wenchuan earthquake. *J. Geophys. Res.*, **114**, A04320, doi: 10.1029/2008JA013698. [Link]

Liu, J. Y., C. H. Chen, Y. I. Chen, W. H. Yang, K. I. Oyama, and K. W. Kuo, 2010a: A statistical study of ionospheric earthquake precursors monitored by using equatorial ionization anomaly of GPS TEC in Taiwan during 2001-2007. *J. Asian Earth Sci.*, **39**, 76-80, doi: 10.1016/j.jseaes.2010.02.012. [Link]

Liu, J. Y., Y. I. Chen, C. H. Chen, and K. Hattori, 2010b: Temporal and spatial precursors in the ionospheric global positioning system (GPS) total electron content observed before the 26 December 2004 M9.3 Sumatra-Andaman Earthquake. *J. Geophys. Res.*, **115**, A09312, doi: 10.1029/2010JA015313. [Link]

Liu, J. Y., H. Le, Y. I. Chen, C. H. Chen, L. Liu, W. Wan, Y. Z. Su, Y. Y. Sun, C. Lin, and M. Q. Chen, 2011: Observations and simulations of seismoionospheric GPS total electron content anomalies before the 12 January 2010 *M*7 Haiti earthquake. *J. Geophys. Res.*, **116**, A04302, doi: 10.1029/2010JA015704. [Link]

Liu, J. Y., Y. I. Chen, C. C. Huang, M. Parrot, X. H. Shen, S. A. Pulinets, Q. S. Yang, and Y. Y. Ho, 2015: A spatial analysis on seismo-ionospheric anomalies observed by DEMETER during the 2008 M8.0 Wenchuan earthquake. *J. Asian Earth Sci.*, **114**, 414-419, doi: 10.1016/j.jseaes.2015.06.012. [Link]

Liu, J. Y., Y. B. Tsai, C. H. Chen, Y. I. Chen, and H. Y. Yen, 2016: Integrated Search for Taiwan Earthquake Precursors (iSTEP). *IEEJ Trans. Fund. Mater.*, **136**, 214-220, doi: 10.1541/ieejfms.136.214. [Link]

Liu, Y. H., C. K. Chao, S. Y. Su, and C. H. Liu, 2012: Study of a coincident observation between the ROCSAT-1 density irregularity and Ascension Island scintillation. *Radio Sci.*, **47**, RS5001, doi: 10.1029/2011RS004908. [Link]

McClure, J. P., S. Singh, D. K. Bamgboye, F. S. Johnson, and H. Kil, 1998: Occurrence of equatorial F region

irregularities: Evidence for tropospheric seeding. *J. Geophys. Res.*, **103**, 29119-29135, doi: 10.1029/98JA02749. [Link]

Minami, S., S. Tsutsumi, and Y. Takeya, 1980: Experimental results of high speed sweeping of the positive ion temperature probe and its application to the ionospheric sounding. *Denki Gakkai Ronbunshi*, **100**, 253-258, doi: 10.1541/ieejfms1972.100.253. [Link]

Nishihashi, M., K. Hattori, H. K. Jhuang, and J. Y. Liu, 2009: Possible spatial extent of ionospheric GPS-TEC and NmF2 anomalies related to the 1999 Chi-Chi and Chia-Yi Earthquakes in Taiwan. *Terr. Atmos. Ocean. Sci.*, **20**, 779-789, doi: 10.3319/TAO.2009.01.22.01(T). [Link]

Ossakow, S. L., 1981: Spread-*F* theories—A review. *J. Atmos. Terr. Phys.*, **43**, 437-452, doi: 10.1016/0021-9169(81)90107-0. [Link]

Oyama, K. I., 1976: A systematic investigation of several phenomena associated with contaminated Langmuir probes. *Planet. Space Sci.*, **24**, 183-190, doi: 10.1016/0032-0633(76)90104-5. [Link]

Oyama, K. I., Y. Kakinami, J. Y. Liu, M. Kamogawa, and T. Kodama, 2008: Reduction of electron temperature in low-latitude ionosphere at 600 km before and after large earthquakes. *J. Geophys. Res.*, **113**, A11317, doi: 10.1029/2008JA013367. [Link]

Pulinets, S. and K. Boyarchuk, 2005: Ionospheric Precursors of Earthquakes, Springer-Verlag Berlin Heidelberg, Berlin, Germany, 315 pp, doi: 10.1007/b137616. [Link]

Rich, F. J., 1994: Users Guide for the Topside Ionospheric Plasma Monitor (SSIES, SSIES-2 and SSIES-3) on Spacecraft of the Defense Meteorological Satellite Program, Volume 1: Technical Description, Environmental Research Papers, No. 1151.

Saroso, S., J. Y. Liu, K. Hattori, and C. H. Chen, 2008: Ionospheric GPS TEC anomalies and M ≥ 5.9 earthquakes in Indonesia during 1993 - 2002. *Terr. Atmos. Ocean. Sci.*, **19**, 481-488, doi: 10.3319/TAO.2008.19.5.481(T). [Link]

Smith, D., 1972: The application of Langmuir probes to the measurement of very low electron temperatures. *Planet. Space Sci.*, **20**, 1717-1726, doi: 10.1016/0032-0633(72)90193-6. [Link]

Su, S. Y., H. C. Yeh, and R. A. Heelis, 2001: ROCSAT 1 ionospheric plasma and electrodynamics instrument observations of equatorial spread *F*: An early transitional scale result. *J. Geophys. Res.*, **106**, 29153-29159, doi: 10.1029/2001JA900109. [Link]

Su, S. Y., H. C. Yeh, C. K. Chao, and R. A. Heelis, 2002: Observation of a large density dropout across the magnetic field at 600 km altitude during the 6-7 April 2000 magnetic storm. *J. Geophys. Res.*, 107, SIA 18-1-SIA 18-9, doi: 10.1029/2001JA007552. [Link]

Su, S. Y., C. H. Liu, H. H. Ho, and C. K. Chao, 2006: Distribution characteristics of topside ionospheric density irregularities: equatorial versus midlatitude regions. *J. Geophys. Res.*, **111**, A06305, doi: 10.1029/2005JA011330. [Link]

Tsai, Y. B., J. Y. Liu, K. F. Ma, H. Y. Yen, K. S. Chen, Y. I. Chen, and C. P. Lee, 2004: Preliminary results of the iSTEP program on integrated search for Taiwan earthquake precursors. *Terr. Atmos. Ocean. Sci.*, **15**, 545-562, doi: 10.3319/TAO.2004.15.3.545(EP). [Link]

Tsyganenko, N. A., 1995: Modeling the Earth's magnetospheric magnetic field confined within a realistic magnetopause. *J. Geophys. Res.*, **100**, 5599-5612, doi: 10.1029/94JA03193. [Link]

Venkatraman, S. and R. Heelis, 1999a: Longitudinal and seasonal variations in nighttime plasma temperatures in the equatorial topside ionosphere during solar maximum. *J. Geophys. Res.*, **104**, 2603-2611, doi: 10.1029/1998JA900109. [Link]

Venkatraman, S. and R. Heelis, 1999b: Effects of solar activity variations on adiabatic heating and cooling effects in the nighttime equatorial topside ionosphere. *J. Geophys. Res.*, **104**, 17117-17126, doi: 10.1029/1999JA900196. [Link]

Wehner, G. and G. Medicus, 1952: Reliability of probe measurements in hot cathode gas diodes. *J. Appl. Phys.*, **23**, 1035-1046, doi: 10.1063/1.1702342. [Link]

Whipple, E. C., 1961: The ion-trap results in "Exploration of the upper atmosphere with the help of the third Soviet Sputnik". NASA Technical Note, D-665, National Aeronautics and Space Administration, Washington.

Yeh, H. C., S. Y. Su, Y. C. Yeh, J. M. Wu, R. A. Heelis, and B. J. Holt, 1999: Scientific mission of the IPEI payload onboard ROCSAT-1. *Terr. Atmos. Ocean. Sci.*, Supplementary Issue, 19-42, doi: 10.3319/TAO.1999.10.S.19(ROCSAT). [Link]

Zuccaro, D. R. and B. J. Holt, 1982: A technique for establishing a reference potential on satellites in planetary ionospheres. *J. Geophys. Res.*, **87**, 8327-8329, doi: 10.1029/JA087iA10p08327. [Link]